Advances in Science and Technology Research Journal

Advances in Science and Technology Research Journal, 2025, 19(11), 258–274
https://doi.org/10.12913/22998624/209018
ISSN 2299-8624, License CC-BY 4.0

Received: 2025.05.30
Accepted: 2025.09.15
Published: 2025.10.01

Geometric personalization of the total human model for safety model to female anthropometry using dual kriging

Dominik Jastrzębski[1]

[1] Faculty of Power and Aeronautical Engineering, Warsaw University of Technology, ul. Nowowiejska 24 00-665 Warsaw, Poland
E-mail: dominik.jastrzebski@pw.edu.pl

ABSTRACT

This paper presents a methodology for geometric personalization of numerical human body models, specifically focusing on adapting the 50th percentile male THUMS model to represent female anthropometry for pedestrian-vehicle collision analysis. Road accidents involving pedestrians represent a significant social and economic problem worldwide, with pedestrians being one of the most vulnerable road users. The study developed a morphing method using the Dual Kriging algorithm to transform the external and internal geometry of the base model while maintaining numerical stability. The process involved using a 3D female surface model as a reference, mapping control points, and ensuring anatomical accuracy especially in the thoracic region. The personalized models were validated through simulated collision tests with a passenger vehicle at 40 km/h, which demonstrated that the models maintained expected kinematic behavior while reflecting the anthropometric differences. Results confirmed that geostatistical algorithms can effectively personalize numerical human models, providing a foundation for future injury analysis considering population diversity.

Keywords: biomechanics, morphing, THUMS, pedestrian safety, vehicle collision, geometric personalization, Dual Kriging, female body model.

INTRODUCTION

Road accidents constitute a significant social and economic problem worldwide. Despite technological progress and the development of safety systems, the number of fatalities and injuries in traffic incidents remains high. Pedestrians are one of the most vulnerable groups of road users. In 2024, Poland recorded 4.719 accidents involving pedestrians (21.9% of all road accidents), resulting in 428 fatalities (22.6% of all road deaths) [1]. In the European context, pedestrians account for 18.4% (3.750) of road fatalities according to the latest Eurostat data for 2023 [2]. It is particularly significant that vehicle-pedestrian collisions are the most common cause of fatalities in this group.

Due to the growing threat to pedestrians, new legal regulations are being introduced, and technologies are being developed to minimize collision consequences. ADAS (Advanced Driver Assistance Systems) used in modern vehicles enable automatic pedestrian detection and emergency braking activation to avoid collisions [3]. These solutions are included in European Union regulations and subject to numerous scientific studies. For example, Benmimoun et al. [4] describe a two-stage safety analysis method for ADAS within the euroFOT project, testing 1.000 vehicles in real traffic conditions. The German Insurance Association [5] presents accident statistics in Germany and the potential of driver assistance systems to reduce their occurrence. Kuehn et al. [6] analyze the effectiveness of ADAS in trucks, showing that AEBS could prevent up to 12% of truck accidents. Papis and Matyjewski [7] demonstrate that AEBS can reduce the number of pedestrian accidents and severe injuries by 40–50%. Park et al. [8] present ADAS testing in a vehicle-in-the-loop

environment using real vehicles and simulation. Waykole et al. [9] evaluate lane detection algorithms for autonomous vehicles, achieving 97–99% accuracy. Lubkowski et al [10] examine driver trust in ADAS and the effectiveness of training, highlighting the need for improved education. Dziewoński et al. [11] describe the Polish aDRIVE project for simulation-based assessment of driving automation systems and ADAS algorithms. Despite these efforts, precise analysis of collision biomechanics and personalization of numerical models remain crucial for further increasing the effectiveness of pedestrian protection systems.

Biomechanical analyses of influence of road accidents on human body can be carried out using three main methods: experiments with ATD (anthropometric test device) test dummies, research on PMHS (post mortem human subject) human cadavers, and computer simulations [12]. Among these, computer simulations are characterized by the greatest flexibility, repeatability, and the ability to analyze various scenarios without conducting costly experiments. Numerical models, such as THUMS (Total Human Model for Safety), allow for advanced biomechanical research and provide a foundation for designing safety systems [13].

While computer simulations offer significant advantages in terms of flexibility and repeatability, it is important to recognize the limitations and sources of discrepancies when comparing their results to those obtained from physical experiments. One of the sources of differences in the results obtained between cadaver tests and computer simulations with the same parameters are geometric differences between the applied model and the cadavers used in the experiment. In the literature, many examples can be found in which scaling of results to a standardized dummy size is used in order to compare outcomes obtained from cadavers of different dimensions. Another approach is the geometric personalization of human models so that the model mesh is as close as possible to the shape of the cadaver in a given test.

Standard numerical human models are based on average anthropometric values, mainly for 50th percentile males. However, accident victims are people with various anatomical characteristics, which can affect their susceptibility to injuries.

There are two approaches to performing such simulations with personalized geometry—morphing of individual body parts and morphing of entire human models. Examples of studies from the first group include works in which single femurs [14, 15], lower limbs [16], the infant head [17], the trabecular bone of the femur [18], the pelvis [19], the thorax [20], the skull [21], or a facial model as a basis for cranio-maxillofacial surgery [21] were morphed. Due to the nature of this study, which places the greatest emphasis on morphing the entire human model, a more detailed review was conducted regarding the morphing of whole models. Although morphing enables a broader and more detailed range of computer simulations, it is not a widely known method. The most frequently morphed model is the GHBMC model, using Kriging [22, 23], the least squares method [23], thin-plate spline interpolation considering material variability [24], radial basis function [25], as well as cases where the method is not specified [26–28]. There are also articles in which the THUMS model is subjected to geometric personalization without specifying the morphing algorithm, including simulations of side impacts [29], the influence of obesity on injuries resulting from frontal collisions [30], and simulations investigating the impact of geometric parameters on side impact outcomes [31]. Additionally, studies are presented in which mesh surface models of children aged 3 to 11 years in the upright position [32] and adults in the seated position [33] are created. Due to the availability of the PIPER Child model, which is provided free of charge, the authors of article [34] used Kriging to morph the child model into an average-sized adult male model. The target shape was defined by the skin contour as well as computed tomography scans of the pelvis and spine.

Studies indicate that women suffer more serious injuries compared to men at similar collision speeds, resulting from, among other things, different body mass distribution, bone structure, and tissue elasticity [35]. Due to these differences, it is necessary to develop methods enabling personalization of numerical models that consider individual anatomical characteristics of different demographic groups.

The aim of this study was to develop a methodology for geometric personalization of the THUMS AM50 male body model to female pedestrian geometry using Dual Kriging method. This work will contribute to improving the quality of biomechanical analyses and designing safety systems that consider actual population diversity.

METHODOLOGY

Selection and preparation of the base model

Dual Kriging (described in detail in [36]) is a curvilinear interpolation method that requires the positions of control points defining the interpolation curve as input data. With the known positions of these control points, it is possible to determine the locations of points in their vicinity. Due to limitations of the method based solely on control points from anthropomorphic measurements in lying position (described in [37]), it was not possible to achieve significant changes in external geometry or control over the internal geometry of the model. To expand the range of models that can be obtained to include female body models and people with anthropometry significantly different from the average male, it was necessary to develop a new method.

Since the Dual Kriging algorithm used in earlier methods demonstrated stability and correct operation, it was retained as the main morphing tool. However, the method of collecting control points was changed – similar to the case of thorax morphing, where the sternum was morphed manually, while ribs were analyzed automatically. In this case, a certain degree of automation was also applied, in contrast to the method described in [37] where points were collected manually.

To create an average female model based on the 50th percentile male model, a free surface model of a female body for 3D animation was used. This model featured a high degree of anthropometric realism with a sparse mesh (4.984 elements). Due to the greater detail of the mesh compared to the THUMS model, the quality of representation was reduced in Blender v. 2.82, removing ears and merging breasts to simulate outer clothing, similar to the THUMS model. The model before and after modifications is shown in Figure 1.

Between the THUMS model and the modified female model, there were differences in units and their initial arrangement with respect to the coordinate system. The proportions of the individual dimensions of the female model were more important than its absolute height, which in the original unit was 67 m. It was determined that the model was made in inches – after conversion, a height of 1.70 m was adopted. The THUMS model is based on millimeters, so after loading into a single program, their sizes required adjustment. At the morphing stage, no strength calculations were performed, so the absolute size of the models did not affect the result. The model was finally scaled to a height of 1.634 m, in accordance with the value for the 50th percentile woman [38].

Procedure scheme

To select characteristic points on the surface of the THUMS model while not limiting to points where anthropometric measurements are collected, the following procedure was developed:

1. Both models were loaded into one space in the Blender program – the female body model in its entirety, while the THUMS model only as its external surface.
2. The surface model of the female body was scaled and arranged so as to resemble the unmodified THUMS model as much as possible.
3. The nodes of the mesh of the enlarged and initially modified female body model were projected onto the surface of the THUMS model.
4. These nodes are used as control points to morph the external surface of the THUMS model.
5. The nodes of the external surface of the THUMS model are used as control points to morph the entire model (not only its external surface).

After going through these five steps, the entire numerical model should take on the desired shape. For a more precise explanation of the method presented, individual sub-points will be discussed separately.

Ad 1: The free Blender program was used to modify the mesh, which enables editing and scaling of selected model fragments. It was decided to export the external surface of the THUMS model to Blender instead of importing the female model mesh into LS-Dyna. All surface nodes were assigned to one group, and then a Matlab script wrote their values to a separate file, which allowed loading only the surface of the model.

Ad 2: After overlaying the models and unifying the units, differences in position and sizes of body parts were noticed. To equalize them, a "bone" system used in 3D animation was applied, which allows manipulating the model by controlling the movement and scaling of selected areas. Nodes closer to the "bone" moved more, and if they were under the influence of several "bones," their movement was the sum of the interactions.

Similarly, "bones" were used to scale the model. The degree of deformation depended on

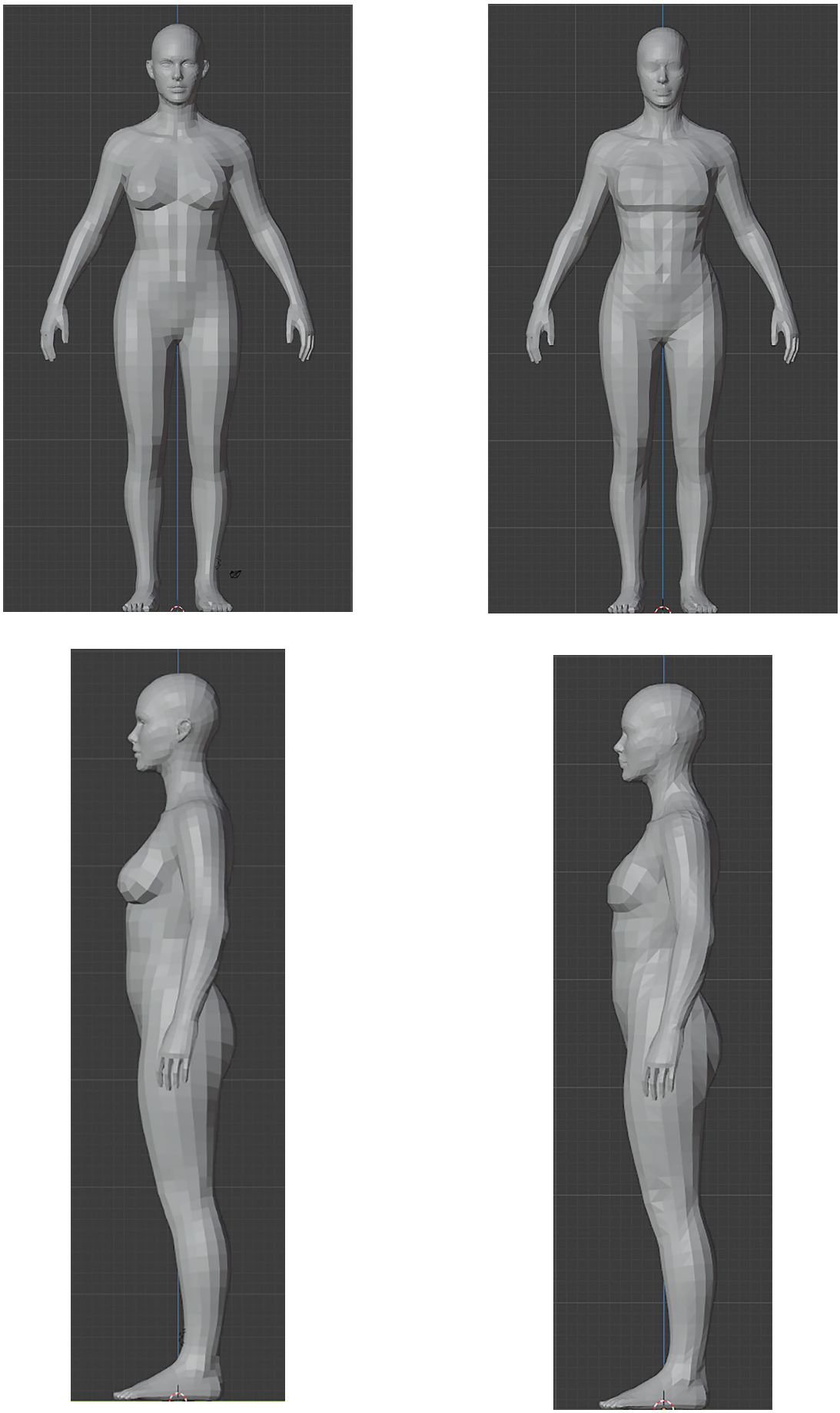

Figure 1. Base surface model of a female body before (left) and after (right) simplification

the distance of nodes from the "bone" and their number. Scaling could be performed in one axis, two planes, or in all three axes simultaneously, which allowed precise adjustment of the model.

To arrange the models in the same way, 20 "bones" were added in key areas, such as legs, pelvis, spine, arms, and head (Figure 2). This made it possible to obtain a model corresponding to the shape of the THUMS model.

Ad 3: To project the mesh nodes of the modified female model onto the surface of the THUMS model, the algorithm looked for the three closest nodes of the THUMS model for each node of the modified model. The distance to all nodes of the THUMS model was calculated, and then the three closest ones were determined, which defined the reference plane.

Based on the vectors created from these three points, the normal vector to the plane was calculated, which made it possible to determine the projection of the node. This process was repeated for all nodes of the modified model to obtain the best possible fit to the THUMS model mesh. This made it possible to project onto the approximate mesh, despite differences in the number and shape of elements of both models.

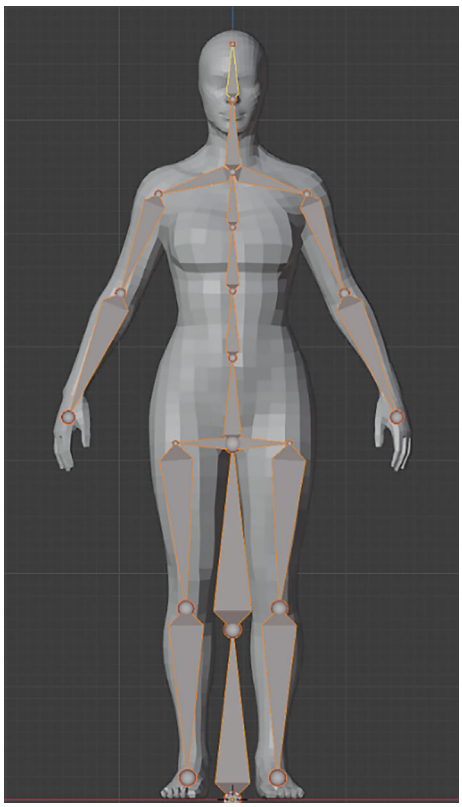

Figure 2. „Bones" used for local scaling of a female body surface

A graphical presentation of the method is shown in Figure 3, while the mathematical description of the method presented is as follows: Input data:

$$K_i = \left(x_k^i, y_k^i, z_k^i\right) \tag{1}$$

$$T = \begin{bmatrix} T_1 \\ \vdots \\ T_n \end{bmatrix} = \begin{bmatrix} x_T^1 & y_T^1 & z_T^1 \\ \vdots & \vdots & \vdots \\ x_T^n & y_T^n & z_T^n \end{bmatrix} \tag{2}$$

$$T - K_i = \begin{bmatrix} x_T^1 - x_k^i & y_T^1 - y_k^i & z_T^1 - z_k^i \\ \vdots & \vdots & \vdots \\ x_T^n - x_k^i & y_T^n - y_k^i & z_T^n - z_k^i \end{bmatrix} \tag{3}$$

$$d(T, K_i) = \\ = \begin{bmatrix} \sqrt{(x_T^1 - x_k^i)^2 + (y_T^1 - y_k^i)^2 + (z_T^1 - z_k^i)^2} \\ \vdots \\ \sqrt{(x_T^n - x_k^i)^2 + (y_T^n - y_k^i)^2 + (z_T^n - z_k^i)^2} \end{bmatrix} \tag{4}$$

From the above matrix, the smallest values and their corresponding nodes are selected:

$$\begin{aligned} T_i^1 &= (x_T^1, y_T^1, z_T^1) \\ T_i^2 &= (x_T^2, y_T^2, z_T^2) \\ T_i^3 &= (x_T^3, y_T^3, z_T^3) \end{aligned} \tag{5}$$

where: K_i – node of the female model mesh projected onto the THUMS model mesh, T_i^1, T_i^2, T_i^3 – nearest nodes of the THUMS model mesh Normal vector to the plane determined by T_i^1, T_i^2, T_i^3:

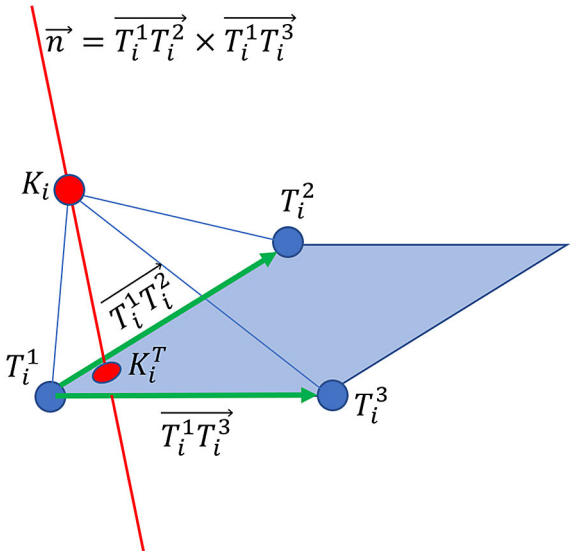

Figure 3. Graphical representation of the applied projection mode

$$\overrightarrow{n} = \overrightarrow{T_i^1 T_i^2} \times \overrightarrow{T_i^1 T_i^3} = \overrightarrow{(n_x, n_y, n_z)} \quad (6)$$

Equation of the plane determined by T_i^1, T_i^2, T_i^3

$$n_x x + n_y y + n_z z - n_x x_T^1 - n_y y_T^1 - n_z z_T^1 = 0 \quad (7)$$

Equation of the normal line to the determined plane presented in parametric form:

$$\begin{aligned} x(t) &= x_k^i + n_x t \\ y(t) &= y_k^i + n_y t \\ z(t) &= z_k^i + n_z t \end{aligned} \quad (8)$$

where: t after inserting the line in parametric form into the plane equation and transformations, is:

$$t = -\frac{n_x(x_k^i - x_T^1) + n_y(y_k^i - y_T^1) + n_z(z_k^i - z_T^1)}{n_x^2 + n_y^2 + n_z^2} \quad (9)$$

After inserting the determined value of t into the parametric form line equations, the calculated values of *x(t), y(t),* and *z(t)* are the coordinates of the projection of point K_i onto the plane determined by T_i^1, T_i^2, T_i^3. This process is repeated for each value i $\in$ < 1, n_k >, where n_k is the number of mesh nodes projected onto the THUMS model. To avoid inaccuracies related to the small distance between hand nodes and torso nodes – the hands of the modified model were projected onto the hands of the THUMS model separately.

Ad 4: The set of points does not constitute a ready mesh, but a projection of the female surface model points onto the THUMS model mesh. This determined the positions of the female model mesh nodes, which enabled morphing of the THUMS model surface. Morphing of the entire model was not applied due to numerical complexity and limited control over the process. The set included 1.184 points for hands and 3.135 for the rest of the body. Control points in their initial and final positions are shown in Figure 4. The obtained mesh was automatically smoothed in Blender, and individual nodes were manually corrected to ensure anatomical correctness. The resulting surface model can be the basis for further morphing. Hands and the rest of the body appear as separate models, and their connection takes place in the next step, eliminating errors in morphing the entire model simultaneously. This division avoided deformation of the chest and sides of the torso.

Ad 5: Finally, the nodes from point 4 were used as control points to complete the model. Separate sets of nodes were assigned to morphing the torso and hands. Due to the high number of nodes (50,500), only 25% were used as control points, which enabled morphing of the torso without hands.

To precisely fit the arms, a multi-stage selection of control points was necessary. Not only was the external shape considered, but also the alignment of the head of the humerus with the joint and the connecting surfaces of the hand with the torso. To prevent mesh penetration, key nodes were selected: internal humeral, forearm, and hand socket, hand-torso connections, and the inner part of the arm and armpit.

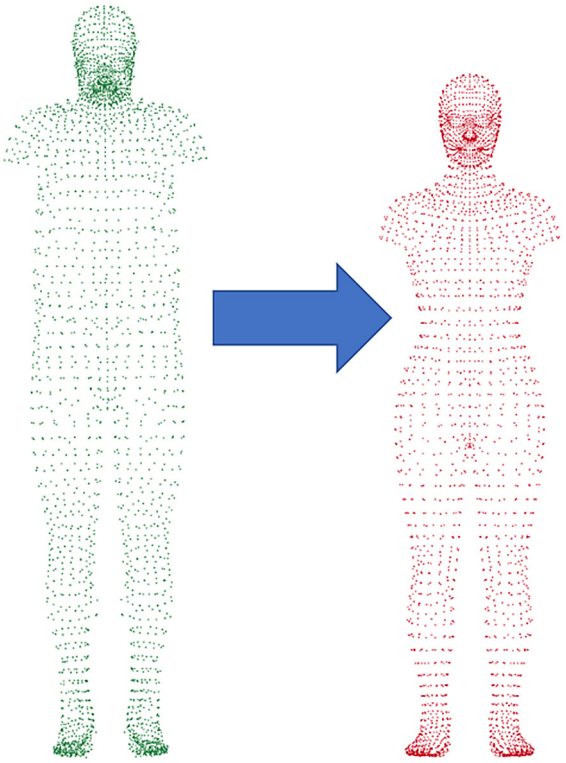

Figure 4. Control points used for morphing the external surface

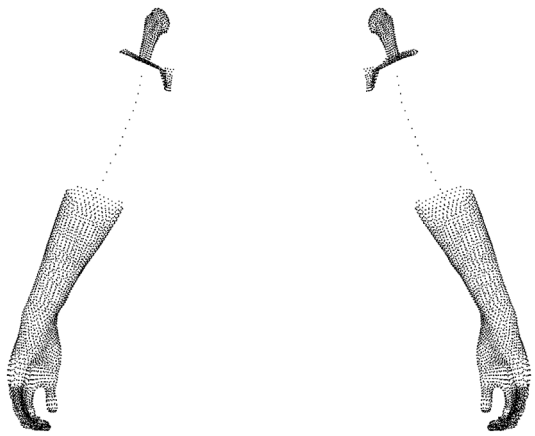

Figure 5. Control points used for arms morphing

After morphing, hands adapted to the upper limbs of the surface model were obtained, without mesh penetration and consistent with the skeletal system, used control points shown in Figure 5. However, after merging the model, an error in the chest morphing was detected.

Re-morphing the thorax

When selecting control points for torso morphing, they were placed on the external surface of the model, which allowed maintaining the proportions of the skeletal system relative to the external body dimensions. This method worked for small changes, such as adaptation to slight overweight or underweight, but larger modifications led to unnatural skeletal proportions [37].

In the case of the female model, control points placed on the outside caused the chest to adapt to the surface shape, while maintaining proportions relative to the male model. The result was an unnatural bending of the sternum and ribs in the breast area (Figure 6).

To eliminate these irregularities, it was necessary to repeat the morphing process, adding modifications only to the thorax. The starting point is the external surface of the THUMS model adapted to the female model. Then the thorax, consisting of ribs, sternum, vertebrae, discs, ligaments, and intercostal muscles, was modified based on specially selected nodes serving as control points.

Initially, it was planned to use chest X-rays from the PadChest database, but the great anatomical diversity made it impossible to choose a single pattern. Instead, priority became the numerical stability of the model. The selection of control points minimized the risk of instability while maintaining the geometric structure of the model. Figure 7 shows the control points for thorax morphing, selected so that its size was the result of morphing the space around it, not direct modification. Points on the abdomen, back, and sides of the torso were considered, which allowed adapting the shape of the spine and ribs. To account for anatomical differences in the waist, control points were added in its area and the surface connecting the waist with the armpits. Points on the shoulders, collarbones, and neck enabled obtaining a coherent model surface.

With such selected points, thorax morphing was performed, which adapted it to the external surface of the THUMS model, eliminating deformations. Figure 8 shows a comparison of the thorax before and after morphing. Then the entire morphing process for the remaining parts of the model was repeated, taking into account all thorax points as control points. In this way, the final shape of the female body model was obtained, which can be the basis for further modifications and for creating subsequent models with a higher degree of personalization (Figure 9).

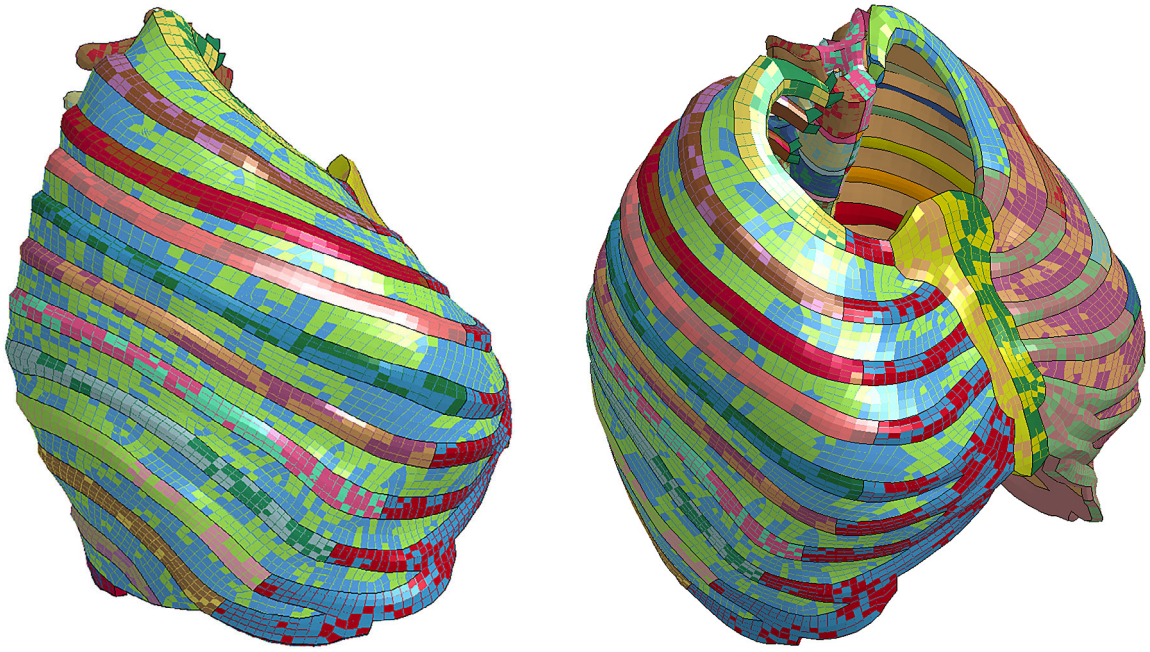

Figure 6. Lateral and isometric views of an incorrectly morphed female thorax

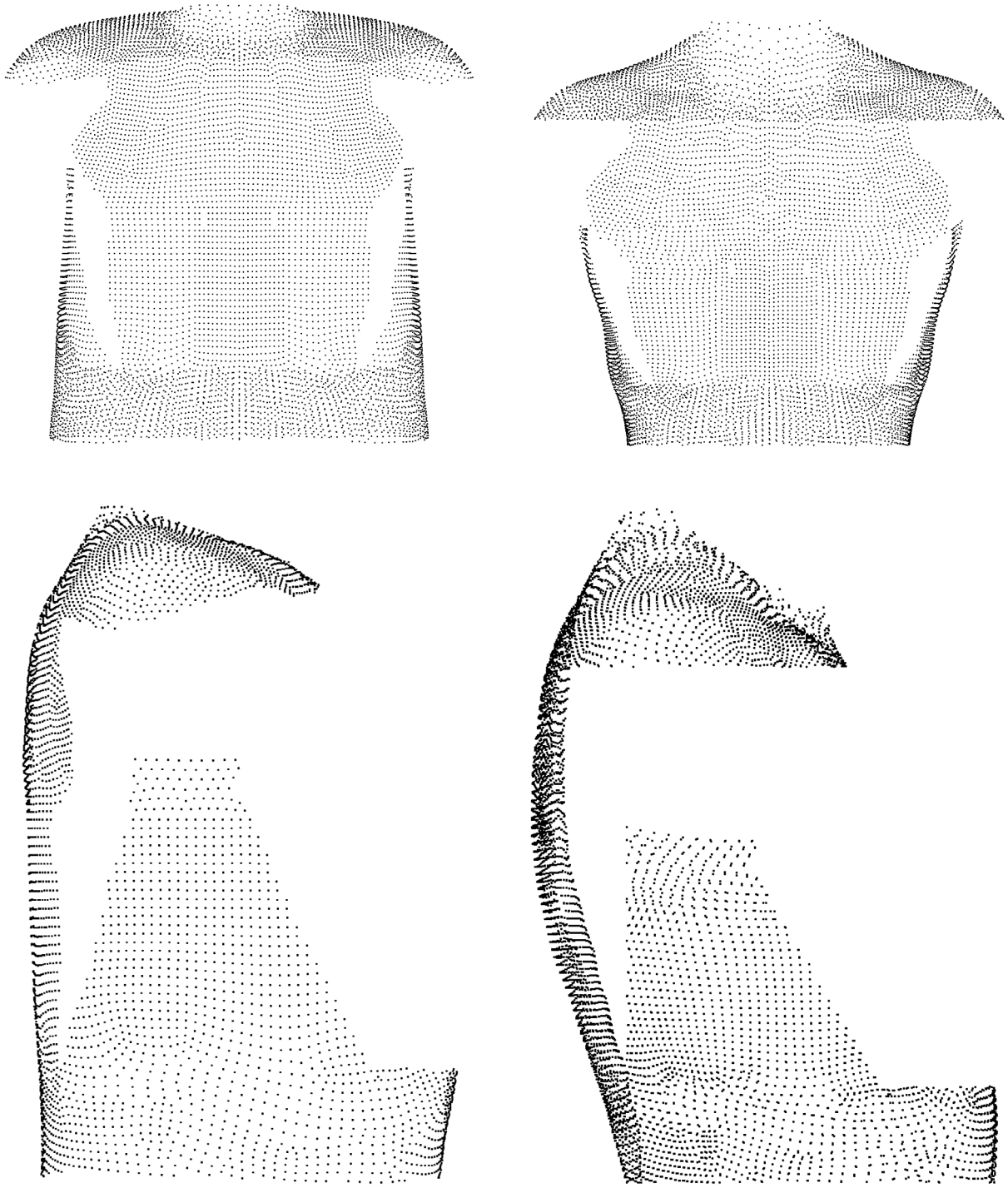

Figure 7. Control points selected for morphing the thorax on the THUMS model (left) and the female model (right)

RESULTS

After the morphing was completed, it was necessary to check whether the models obtained in this way are numerically stable and whether the results obtained with them are consistent with experimental results. The available and at the same time basic model, on which the methods described in this paper were based, was a numerical model of a human in a standing position, so tests checking the correctness of the model's operation after numerical operations performed on it were chosen as tests for pedestrian-vehicle collisions.

Since the aim of the work was not to replicate collision tests, but to verify the correctness of the morphing process, simplified model tests were

decided upon. Literature [39] states that in 11% of pedestrian-vehicle collision cases, the legs were parallel, and in 6% parallel and separate. This is a position similar to the obtained models, so it was used for testing.

Most literature tests include a position with one leg extended forward, so the analysis focuses on the kinematics of the head and thorax, which are consistent with the reference tests. The position of the legs during impact has little effect on the model's kinematics, as tendons in the knees often rupture, and the legs adapt to the shape of the vehicle [40]. Figure 15 shows that the leg on the car side bends unnaturally, while the upper body remains motionless. Due to the different behavior of the leg further from the vehicle (Figure 10 c), the lower part of the body model was not compared with literature data.

To perform the described test, a ready-made model of a Honda Accord car made available in 2016 by NHTSA was used. The model consists of 1,941,659 elements, 1,969,784 nodes, and

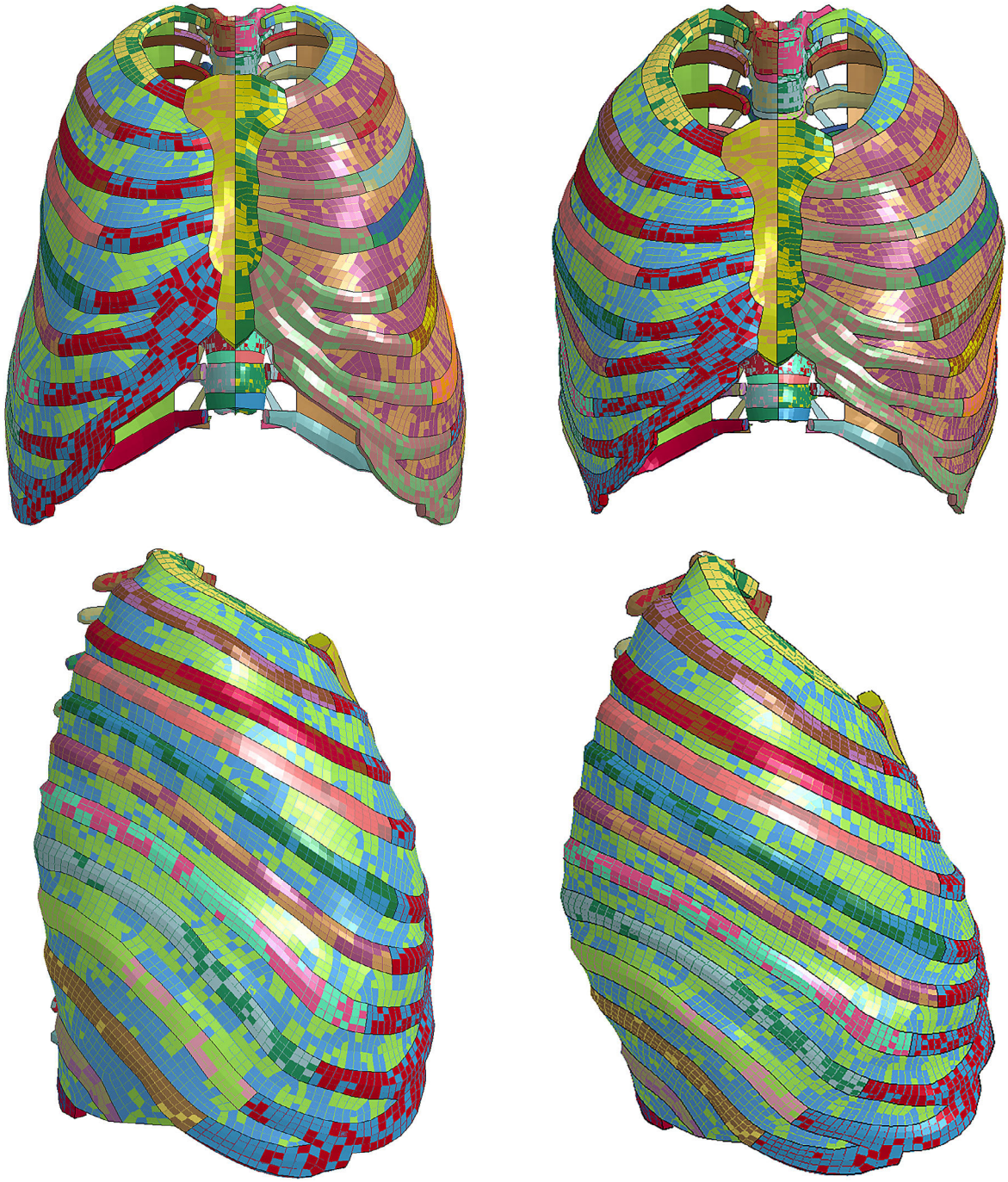

Figure 8. Comparison of thoraxes before morphing (left) and after morphing (right)

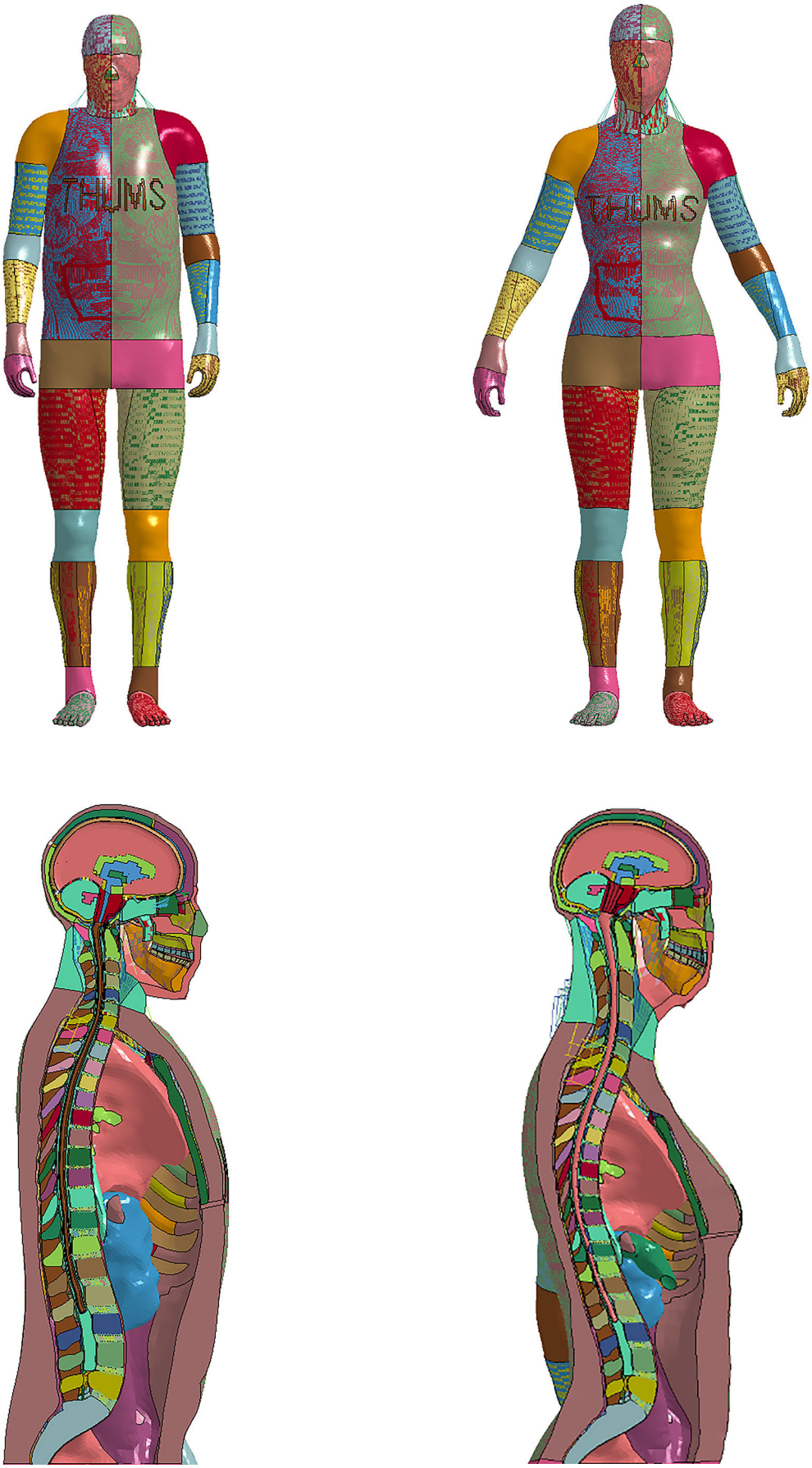

Figure 9. Comparison of models before morphing (THUMS model on the left) and after morphing (female body model on the right)

1.054 parts. Its mass is 1668.2 kg and is 7.2 kg heavier than its real counterpart (Honda Accord LX 4-door sedan). The wheelbase of the model is 2799 mm, which is 5 mm more than the base car. The model is presented in Figure 11.

Collision tests were conducted on the female model obtained by morphing the THUMS base model. Simulations were performed in LS-DYNA software, applying initial conditions corresponding to real collision experiments:

- vehicle speed: 11.1 m/s (40 km/h),
- surface contact between model and vehicle (AUTOMATIC_SURFACE_TO_SURFACE function),
- friction coefficient: 0.2,
- model positioned with right side to the approaching vehicle.

During the simulation setup, gravitational field stabilization was not applied. This decision was made because the primary objective of the test was to validate the numerical model itself, its numerical stability and potential issues resulting from the performed morphing process.

First, the results of a passenger car collision with a fiftieth percentile male model are presented. This was the base THUMS AM50 v4.01 model without modifications, with the collision conditions described above. Graphs in the form of trajectory of head motion, T1 and T8 vertebrae, in a moving reference frame associated with the car are presented in Figure 12. The next tested model was the female body model in a collision with a passenger car. As in the case of previous simulations – first the trajectory of the head, then the T1 and T8 vertebrae (Figure 13) will be presented.

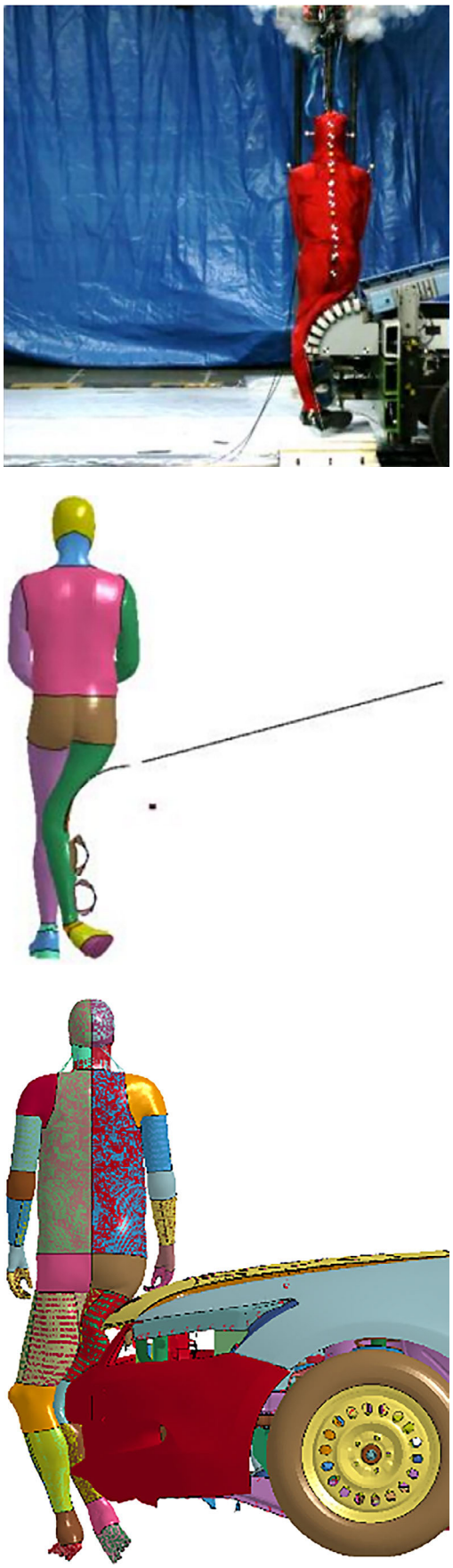

Figure 10. Comparison of model positions in the baseline simulation (c) with the cadaver test (a) and the simulation from the literature (b) [41]

DISCUSSION

Limitations of the presented methods

In computer simulations, simplifications are necessary to obtain realistic results with acceptable calculation time. With technological development, the accuracy of body geometry representation grows thanks to greater computing power. However, even modern computers encounter limitations resulting from errors in estimating material properties [42] or inaccurate geometry obtained, for example, from magnetic resonance imaging [43]. The presented shape personalization methods focused on mapping geometry with

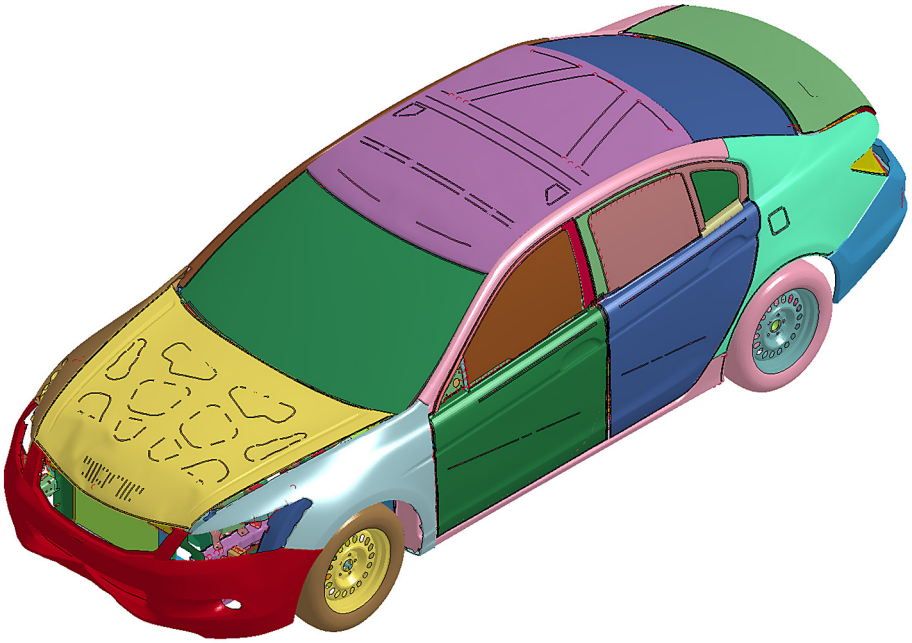

Figure 11. Isometric view of Honda Accord used for validation tests

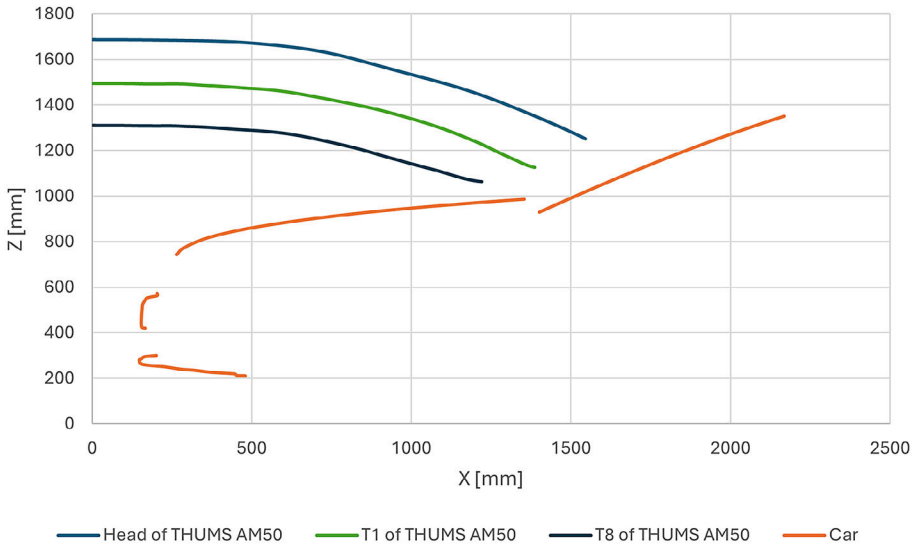

Figure 12. Plot of the trajectories of characteristic parts of the baseline model in the ZX plane relative to the vehicle

a stable computational mesh. The main limitation was the invariability of the model's material properties, which resulted from the lack of available data. Considering variable materials depending on age, sex, and lifestyle remains an issue for future research. Morphing models with different anthropometry, using the same material data, was a simplification. The distribution of adipose tissue, affecting the stiffness of external layers, differs even within the same sex [44–46]. Also, the average thickness of cortical bone in male and female models was a simplification [47]. However, since the THUMS model has been validated and is widely used, maintaining uniform materials allows obtaining comparable results and assessing morphing quality.

Discussion of collision test results of complete human models

Simulation tests of a car model colliding with a numerical human model aimed to assess the

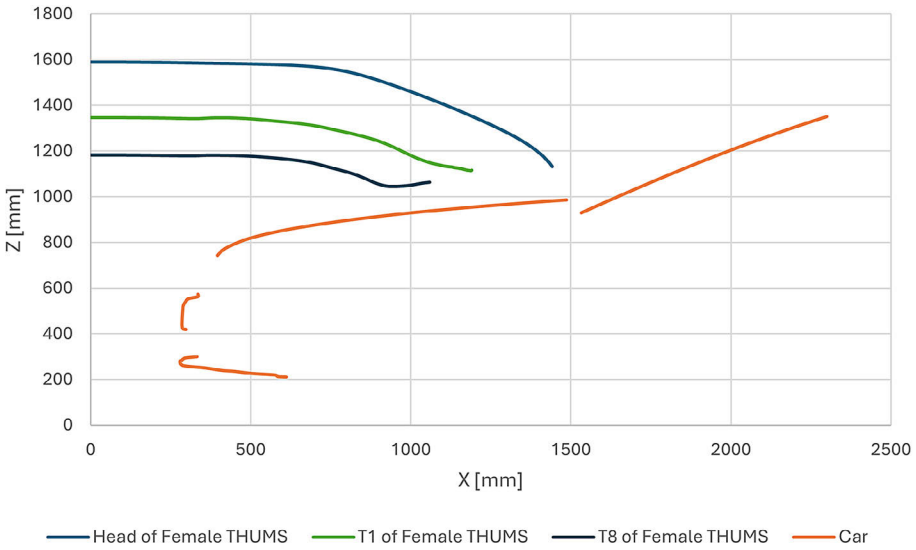

Figure 13. Plot of the trajectories of characteristic parts of the female model in the ZX plane relative to the vehicle

correctness of morphing and numerical stability of the models. This stability is crucial for the quality of data obtained in simulations.

Due to differences in leg positioning between the numerical model and experiments from literature, only the trajectories of the head, T1 and T8 vertebrae were compared. The character of the graphs is consistent with literature [48], where the initial phase of the trajectory is flattened due to body inertia at vehicle speed.

The simulation results demonstrate convergence with findings from Wdowicz and Ptak [49], who provided a comprehensive review of numerical approaches to pedestrian impact simulation, confirming the validity of finite element models through comparison with experimental data and their applicability in forensic investigations. The kinematic characteristics were also consistent with other studies that extensively discuss collisions between vulnerable road users (VRUs) and vehicles [50,51]. The taller model shows a more flattened head trajectory, while in the shorter model, the trajectory curves downward to a greater extent. This is best visible in the case of the T8 vertebra trajectory, which in the base model has a course similar to the head, with slight flattening at the end. The female model, due to a narrower chest and waist, continues rotational movement

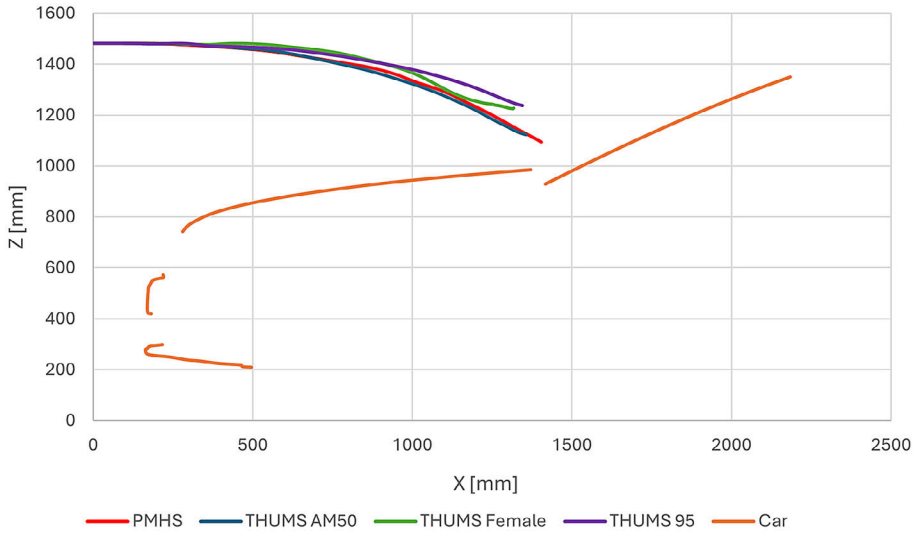

Figure 14. Comparative plot of the T1 vertebra trajectories of the human model and PMHS in the ZX plane relative to the vehicle

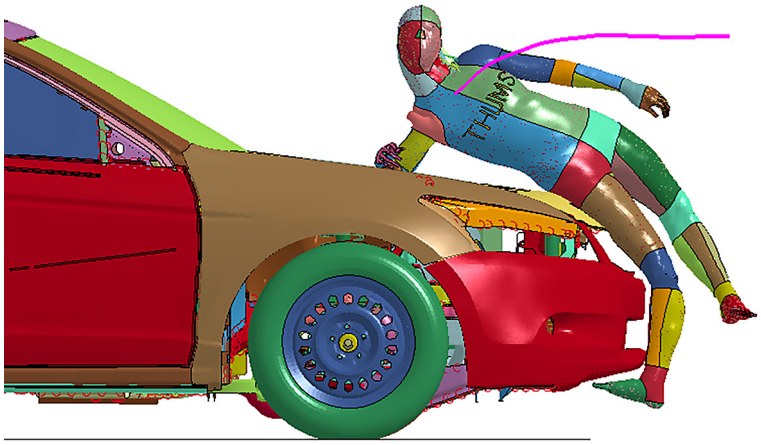

Figure 15. Moment of trajectory change of the T1 and T8 vertebrae in the collision simulation of the female model

longer after the knees contact the bumper. However, its lower height causes earlier contact of the chest with the hood, changing the rebound angle. These differences in T8 and T1 vertebrae trajectories are the effect of the modified model geometry. To ensure clarity in comparisons, test results are normalized to the dimensions of a 50th percentile male dummy as per the SAE J2782 standard. Visible on Figure 14 scaled results of THUMS 95, are the results of a model morphed similarly to the method described in [37].

Comparing the results to literature data, all trajectories were similar, with the base model achieving the most accurate representation. This results from the greatest anthropometric similarity to the reference THUMS AM50 mannequin. Models with changed anthropometry showed different trajectories, which demonstrates the influence of geometry on movement dynamics.

Similarly, in the case of the T1 vertebra, the base model most faithfully reproduced experimental data (Figure 14), while the THUMS 95 model trajectory was the most flattened. The female model showed a slight deviation in trajectory, and its hips were "bounced" by the hood, causing a characteristic change in movement direction. In the subsequent phase, a noticeable sharpening of the trajectory toward the mask is observed, which can be explained in accordance with the pendulum analogy. However, a distinct rebound and displacement of the T1 vertebra along the mask toward the center of the windshield is then visible on the trajectory.

To explain this phenomenon, it is necessary to refer to the animation, a characteristic frame of which is presented in Figure 15. The trajectory marked in the figure represents the path of motion of the T1 vertebra, while the moment at which the animation was paused corresponds to the instant after which a change in the trend of the characteristic occurs. The reason for this is the elbow, which at this point in the simulation rests on the engine hood, while maintaining a right angle relative to the torso. As a result, instead of placing the hand on the hood, the force from it is transmitted along the humerus and clavicle to the chest, and from there to the T1 vertebra, causing a change in the direction of movement and the visible "rebound" on the trajectory plot.

CONCLUSIONS

The obtained results confirm the numerical stability of the model after modifications, allowing for collision simulation without additional stabilization. The visible differences in trajectories result solely from changes in geometry. The focus was not on faithful reproduction of cadaver tests, but on simplified replication while maintaining basic conditions. The introduced simplifications included, among others, hand positioning, which in experimental tests are tied to avoid anomalies in the trajectory. Despite the influence of their position on vertebrae movement, personalized models maintain kinematics similar to experimental studies. Head trajectories and movement until elbow contact with the hood show the same character as in the studies.

The models can serve as a basis for further personalization, taking into account individual material properties. Additionally, they enable

analysis of how geometry influences biomechanical injury indicators. The key conclusion from the presented work is that it is possible to apply geostatistical algorithms, in particular Dual Kriging, for effective geometric personalization of numerical human models. The presented method was limited only to the THUMS AM50 v4.01 model due to the availability of this model, but it is not reserved only for this model. All used scripts are based directly on numerical meshes in text format, without excluding other human body models. At no point in the work were the ordering properties of the base model mesh used, so this method can be applied to other numerical human models such as GHBMC or VIVA+.

REFERENCES

1. Symon E. Road accidents in Poland in 2024. Analytical and Opinion Department of the Road Traffic Bureau of the National Police Headquarters, 2025. (in Polish)
2. Road safety statistics in the EU, Data extracted in March 2025, (Accessed 26.05.2025) https://ec.europa.eu/eurostat/statistics-explained/SEPDF/cache/55846.pdf
3. Antony M. M., Whenish R. Advanced Driver Assistance Systems (ADAS). EAI/Springer Innovations in Communication and Computing, 2021. https://doi.org/10.1007/978-3-030-59897-6_9
4. Benmimoun M., Aust M. Safety Analysis Method for Assessing the Impacts of Advanced Driver Assistance Systems within the European Large Scale Field Test euroFOT. 22nd Enhanced Safety of Vehicles Conference, Washington, DC/USA, 2011.
5. German Insurance Association. Accident statistics and the potential of driver assistance systems. Compact accident research, 2014.
6. Kuehn M., Hummel T., Bende J. Advanced Driver Assistance Systems for Trucks – Benefit Estimation From Real-Life Accidents. Www-Esv.Nhtsa.Dot.Gov, 2011.
7. Papis M., Matyjewski M. Assessment of the influence of the advanced emergency braking systems on pedestrian safety. The Archives of Automotive Engineering – Archiwum Motoryzacji 2017; 77(3): 97–109.
8. Park C., Chung S., Lee H. Vehicle-in-the-loop in global coordinates for advanced driver assistance system. Applied Sciences (Switzerland), 2020. https://doi.org/10.3390/APP10082645
9. Waykole S., Shiwakoti N., Stasinopoulos P. Review on lane detection and tracking algorithms of advanced driver assistance system. Sustainability (Switzerland), 2021. https://doi.org/10.3390/su132011417
10. Lubkowski S. D., Lewis B. A., Gawron V. J. et al. Driver trust in and training for advanced driver assistance systems in Real-World driving. Transportation Research Part F: Traffic Psychology and Behaviour, 2021. https://doi.org/10.1016/j.trf.2021.07.003
11. Dziewoński T., Golon K., Jastrzebski D., et al. From aDrive project to integrated safety. Conference proceedings International Research Council on the Biomechanics of Injury, IRCOBI, 2017.
12. Kalra A., Gupta V., Shen M. et al. Pedestrian safety: An overview of physical test surrogates, numerical models and availability of cadaveric data for model validation. International Journal of Vehicle Safety 2016; 9(1): 39–71. https://doi.org/10.1504/IJVS.2016.077152
13. Toyota Motor Corporation. Documentation Total Human Model for Safety (THUMS) AM50 Pedestrian / Occupant Model, 2011.
14. Bonaretti S., Seiler C., Boichon C. et al. Image-based vs. mesh-based statistical appearance models of the human femur: Implications for finite element simulations. Medical Engineering and Physics, 2014. https://doi.org/10.1016/j.medengphy.2014.09.006
15. Grassi L., Hraiech N., Schileo E. et al. Evaluation of the generality and accuracy of a new mesh morphing procedure for the human femur. Medical Engineering and Physics, 2011. https://doi.org/10.1016/j.medengphy.2010.09.014
16. Klein K. F. Use of parametric finite element models to investigate effects of occupant characteristics on lower-extremity injuries in frontal crashes. ProQuest Dissertations and Theses, 2015.
17. Li Z., Hu J., Zhang J. Comparison of different radial basis functions in developing subject-specific infant head finite element models for injury biomechanics study. ASME 2012 Summer Bioengineering Conference, SBC 2012, 2012. https://doi.org/10.1115/SBC2012-80162
18. Hazrati Marangalou J., Ito K., Cataldi M. et al. A novel approach to estimate trabecular bone anisotropy using a database approach. Journal of Biomechanics, 2013. https://doi.org/10.1016/j.jbiomech.2013.07.042
19. Salo Z., Beek M., Wright D., Marisa Whyne C. Computed tomography landmark-based semi-automated mesh morphing and mapping techniques: Generation of patient specific models of the human pelvis without segmentation. Journal of Biomechanics, 2015. https://doi.org/10.1016/j.jbiomech.2015.01.019
20. Shi X., Cao L., Reed M. P. et al. A statistical human rib cage geometry model accounting for variations

by age, sex, stature and body mass index. Journal of Biomechanics 2014; 47: 2277–2285. https://doi.org/10.1016/j.jbiomech.2014.04.045

21. Teshima T. L., Patel V., Mainprize J. G. et al. A three-dimensional statistical average skull: Application of biometric morphing in generating missing anatomy. Journal of Craniofacial Surgery, 2015. https://doi.org/10.1097/SCS.0000000000001869
22. Beillas P., Berthet F. An investigation of human body model morphing for the assessment of abdomen responses to impact against a population of test subjects. Traffic Injury Prevention 2017; 18(S1): S142–S147. https://doi.org/10.1080/15389588.2017.1307971
23. Lafon Y., Petit P., Beillas P. Comparison of Kriging and Moving Least Square Methods to Change the Geometry of Human Body Models. Stapp Car Crash Journal 2015; 59(November): 337–357.
24. Schoell S. L., Weaver A. A., Urban J. E. et al. Development and validation of an older occupant finite element model of a mid-sized male for investigation of age-related injury risk. SAE Technical Papers 2015; 59(November): 359–383. https://doi.org/10.4271/2015-22-0014
25. Vavalle N. A., Schoell S. L., Weaver A. A. et al. Application of radial basis function methods in the development of a 95th percentile male seated FEA model. Stapp Car Crash Journal, 2014.
26. Zhang K., Cao L., Fanta A. et al. An automated method to morph finite element whole-body human models with a wide range of stature and body shape for both men and women. Journal of Biomechanics, 2017. https://doi.org/10.1016/j.jbiomech.2017.06.015
27. Hu J., Zhang K., Reed M. P. et al. Frontal crash simulations using parametric human models representing a diverse population. Traffic Injury Prevention 2019; 20(sup1): S97–S105. https://doi.org/10.1080/15389588.2019.1581926
28. Miyazaki Y., Railkar A., Awamori S., Kokeguchi A., Amamori I., Katagiri M. Y. Stature and Body Shape Effects on Driver Injury Risks in Frontal Crashes: A Parametric Human Modelling Study. IRCOBI Conference 2017: 284–295.
29. Hwang E., Hu J., Reed M. P. Validating diverse human body models against side impact tests with post-mortem human subjects. Journal of Biomechanics, 2020. https://doi.org/10.1016/j.jbiomech.2019.109444
30. Shi X., Cao L., Reed M. P. et al. Effects of obesity on occupant responses in frontal crashes: a simulation analysis using human body models. Computer Methods in Biomechanics and Biomedical Engineering 2015. https://doi.org/10.1080/10255842.2014.900544
31. Hwang E., Hu J., Chen C. et al. Development, Evaluation, and sensitivity analysis of parametric finite element whole-body human models in side impacts. Stapp Car Crash Journal 2016; 60(November): 473–508.
32. Park B. K., Reed M. P. Parametric body shape model of standing children aged 3–11 years. Ergonomics, 2015. https://doi.org/10.1080/00140139.2015.1033480
33. Park B. K. D., Jones M. L. H., Ebert S., Reed M. P. A parametric modeling of adult body shape in a supported seated posture including effects of age. Ergonomics, 2021. https://doi.org/10.1080/00140139.2021.1992020
34. Liu S., Beillas P., Ding L., Wang X. Morphing an existing open source human body model into a personalized model for seating discomfort investigation. SAE Technical Papers, 2020. https://doi.org/10.4271/2020-01-0874
35. Leo C., Rizzi M. C., Bos N. M. et al. Are there any significant differences in terms of age and sex in pedestrian and cyclist accidents? Frontiers in Bioengineering and Biotechnology, 2021. https://doi.org/10.3389/fbioe.2021.677952
36. Trochu F. A contouring program based on dual kriging interpolation. Engineering with Computers 1993; 9(3): 160–177. https://doi.org/10.1007/BF01206346
37. Poulard D., Chen H., Crandall J. R. et al. Component-level Biofidelity Assessment of Morphed Pedestrian Finite Element Models. IRCOBI Conference, Lyon, 2015: 577–593.
38. Jarosz E. Atlas of Human Measurements. Data for Design and Ergonomic Assessment, 2020. (in Polish).
39. Jastrzębski D., Perz R. Rib kinematics analysis in oblique and lateral impact tests. Acta of Bioengineering and Biomechanics, 2020. https://doi.org/10.5277/ABB-01431-2019-03
40. Song E., Petit P., Trosseille X. et al. New reference PMHS tests to assess whole-body pedestrian impact using a simplified generic vehicle front-end. SAE Technical Papers 2017; 61(November): 299–354. https://doi.org/10.4271/2017-22-0012
41. Song E., Petit P., Uriot J. Modelling of an adjustable generic simplified vehicle for pedestrian impact and simulations of corresponding reference PMHS tests using the GHBMC 50th percentile male pedestrian simplified model. SAE Technical Papers 2018; 2019-Novem(November): 443–487. https://doi.org/10.4271/2018-22-0013
42. Duprez M., Bordas S. P. A., Bucki M. et al. Quantifying discretization errors for soft tissue simulation in computer assisted surgery: A preliminary study. Applied Mathematical Modelling 2020; 77: 709–723. https://doi.org/10.1016/j.apm.2019.07.055
43. Campanelli V., Howell S. M., Hull M. L. Morphological errors in 3D bone models of the distal femur and proximal tibia generated from magnetic

resonance imaging and computed tomography determined using two registration methods. Computer Methods in Biomechanics and Biomedical Engineering: Imaging and Visualization, 2020. https://doi.org/10.1080/21681163.2018.1559101

44. Bose K. Age trends in adiposity and central body fat distribution among adult white men resident in Peterborough, East Anglia, England. Collegium Antropologicum, 2002.
45. Rahman M., Temple J. R., Breitkopf C. R., Berenson A. B. Racial differences in body fat distribution among reproductive-aged women. Metabolism: Clinical and Experimental, 2009. https://doi.org/10.1016/j.metabol.2009.04.017
46. Kirchengast S., Huber J. Fat distribution patterns in young amenorrheic females. Human Nature 2001; 12(2): 123–140. https://doi.org/10.1007/s12110-001-1020-z
47. Jepsen K. J., Bigelow E. M. R., Schlecht S. H. Women build long bones with less cortical mass relative to body size and bone size compared with men. Clinical Orthopaedics and Related Research, 2015. https://doi.org/10.1007/s11999-015-4184-2
48. Yang D. Spatial prediction using kriging ensemble. Solar Energy 2018; 171: 977–982. https://doi.org/10.1016/j.solener.2018.06.1051
49. Wdowicz D., Ptak M. Numerical Approaches to Pedestrian Impact Simulation with Human Body Models: A Review. Archives of Computational Methods in Engineering 2023; 30:4687–4709. https://doi.org/10.1007/s11831-023-09949-2
50. Salgado A., Wdowicz D., et al. Assessing head injury risks in electric scooter accidents: A multi-body simulation study with insights into sex differences. Legal Medicine 2024; 71. https://doi.org/10.1016/j.legalmed.2024.102526
51. Shang S., Masson C., et al. The predictive capacity of the MADYMO ellipsoid pedestrian model for pedestrian ground contact kinematics and injury evaluation. Accident Analysis and Prevention 2021; 149; https://10.1016/j.aap.2020.105803